

Research



Cite this article: Stavenga DG, van der Kooij CJ, Wilts BD. 2017 Structural coloured feathers of mallards act by simple multilayer photonics. *J. R. Soc. Interface* **14**: 20170407. <http://dx.doi.org/10.1098/rsif.2017.0407>

Received: 1 June 2017

Accepted: 7 July 2017

Subject Category:

Life Sciences – Physics interface

Subject Areas:

biomaterials, biophysics

Keywords:

animal coloration, sexual dichromatism, melanin, finite-difference time-domain, iridescence

Author for correspondence:

Doekele G. Stavenga

e-mail: d.g.stavenga@rug.nl

Electronic supplementary material is available online at <https://dx.doi.org/10.6084/m9.figshare.c.3827917>.

Structural coloured feathers of mallards act by simple multilayer photonics

Doekele G. Stavenga¹, Casper J. van der Kooij² and Bodo D. Wilts³

¹Computational Physics, Zernike Institute for Advanced Materials, University of Groningen, 9747 AG Groningen, The Netherlands

²Department of Ecology and Evolution, University of Lausanne, 1015 Lausanne, Switzerland

³Adolphe Merkle Institute, University of Fribourg, Chemin des Verdiers 4, 1700 Fribourg, Switzerland

ORCID DGS, 0000-0002-2518-6177; CvdK, 0000-0003-0613-7633; BDW, 0000-0002-2727-7128

The blue colours of the speculum of the mallard (*Anas platyrhynchos*), both male and female, and the green head feathers of the male arise from light interacting with stacks of melanosomes residing in the feather barbules. Here, we show that the iridescent colours can be quantitatively explained with an optical multilayer model by using a position-dependent effective refractive index, which results from the varying ratio of melanin and keratin. Reflectance spectra obtained by multilayer modelling and three-dimensional finite-difference time-domain calculations were virtually identical. The spectral properties of the barbules' photonic structures are sensitive to variations in the multilayer period and the cortex thickness, but they are surprisingly robust to variations in the spatial parameters of the barbules' melanosome stacks. The blue and green reflectance spectra of the structural-coloured feathers correspond with the sensitivity spectra of the short- and middle-wavelength-sensitive photoreceptors, indicating their biological significance for intraspecific signalling.

1. Introduction

The bright pattern of coloured plumage featured by numerous bird species is important for intraspecific communication and camouflage. The colours can have a pigmentary or structural origin, or the two coloration mechanisms act in concert [1–3]. Pigmentary coloration can be due to various pigments, notably carotenoids and melanin. As carotenoids strongly absorb in the blue to green wavelength range, they cause yellow, orange or red feathers [4]. Melanin pigment, nearly universally found as an animal colorant, absorbs throughout the visible wavelength range and thus causes duller colours [5,6]. Melanin exists in two main forms: eumelanin, which is responsible for grey to black colours, and pheomelanin, which can produce golden to rusty-red colours; intermediate colours result when the two melanins occur as a mixture [7].

Remarkably, in the barbules of many bird feathers, melanin is deposited in special organelles, the so-called melanosomes, which cause structural colours when embedded in regular, nanoscale patterns in a matrix of the feather's keratin [8,9]. Durrer [9] performed extensive transmission electron microscopy (TEM) studies of the feather barbules of numerous bird species and thus found a large variety in the detailed structure of the melanosomes as well as in their spatial arrangements. He interpreted the observed structural colours to be due to the melanosome stacks acting as optical multilayers.

Previous work on the structural-coloured barbules of the bird of paradise *Parotia lawesii* confirmed this view. The reflectance spectra of both the breast and occipital feathers could be explained in detail by applying multilayer theory as well as finite-difference time-domain (FDTD) modelling, using the wavelength-dependent complex refractive indices of keratin and melanin determined with Jamin–Lebedeff interference microscopy [10–13].

Another well-known example of bird species with prominent structurally coloured feathers is the common wild duck or mallard, *Anas platyrhynchos*.

The male has green head feathers and both sexes have blue speculum feathers (wing patches), due to barbules containing stacks of tightly packed melanosomes, enveloped by a keratin cortex [9,14–17]. The arrangement of the melanosomes approximates a hexagonal lattice and therefore it was suggested that the melanosomes optically behave as a two-dimensional photonic crystal rather than as a multilayer [16]. This view was underscored by comparing experimentally measured reflectance spectra with calculated spectra [16,17].

Here, we reinvestigate the optics and anatomy of mallard feather coloration. We combine multilayer modelling with three-dimensional FDTD calculations and thus demonstrate that optical multilayer theory is fully adequate for explaining the coloration of mallard feathers. Comparing the reflectance spectra of the structural coloured feathers with the sensitivity spectra of the mallard's visual photoreceptors shows a striking spectral correspondence.

2. Material and methods

2.1. Animals

Moulted mallard feathers were collected in a location known to be inhabited by a duck community, and were taken from a road kill and a specimen provided by a local huntsman.

2.2. Light microscopy

Photographs of barbules in an intact speculum feather were made with an Olympus SZX16 stereomicroscope, and images of the upper- and undersides of an isolated barbule were made with a Zeiss Universal Microscope (Zeiss, Oberkochen, Germany).

2.3. Transmission electron microscopy

The barbule anatomy was investigated by TEM using standard methods [18]. Briefly, a feather piece was subjected to a series of dehydrations in increasing concentrations of EtOH:H₂O mixtures, embedded in EPON resin and cut to approximately 50 nm sections using a diamond ultramicrotome. Sections were stained using 2% aqueous uranyl acetate solution and examined with a Hitachi 7100 TEM.

2.4. Spectroscopy

Reflectance spectra of both sides of isolated barbules attached to the tip of a glass micropipette were measured with a microspectrophotometer (MSP), which consisted of a Leitz Ortholux microscope (Leitz, Wetzlar, Germany) connected to an AvaSpec 2048–2 CCD detector array spectrometer (Avantes, Apeldoorn, The Netherlands) and a xenon arc light source. The microscope objective was an Olympus 20×, NA 0.46 (Olympus, Tokyo, Japan). Owing to the glass optics, the MSP spectra were limited to wavelengths greater than 350 nm. The area measured with the MSP was a square with edge length of 5–10 μm. The reference was a white diffuse reflectance tile (Avantes WS-2); when the measured object is not diffuse but directionally reflecting this causes severely overestimated reflectance values (by about a factor of 4). Transmittance spectra of isolated barbules, immersed in immersion oil (refractive index 1.515), were also measured with the MSP. Reflectance spectra from intact feathers were measured with a bifurcated reflection probe (Avantes FCR-ZUV200), using also the white diffuse reflectance tile as a reference. The light source was a

deuterium-halogen lamp (AvaLight-D(H)-S). The bifurcated probe illuminated an area with a diameter of about 1 mm, and captured the light reflected in a small spatial angle with aperture about 20°.

2.5. Imaging scatterometry

For investigating the spatial reflection characteristics of the barbules, we performed imaging scatterometry. A small feather piece attached to a glass micropipette was positioned at the first focal point of the ellipsoidal mirror of an imaging scatterometer. The scatterograms were obtained by focusing a white light beam with a narrow aperture (less than 5°) onto a small circular area (diameter approx. 13 μm) of the feather piece, and the spatial distribution of the far-field scattered light was monitored. A flake of magnesium oxide served as a white diffuse reference object (for further details, see [19–21]).

2.6. Modelling

Using parameter values inspired by anatomy, we calculated the reflectance and transmittance spectra of model barbules with a transfer-matrix program, written in Matlab, based on classical optical multilayer theory [20]. The model barbules contained two stacks of melanosomes, embedded in a keratin matrix and enveloped by a keratin cortex. We sliced the melanosomes stacks into 1 nm thin layers and calculated the volume fractions of the components keratin and melanin, f_k and f_m , of each layer, with $f_k + f_m = 1$. The real parts of the wavelength-dependent refractive indices of the two components, n_k and n_m , were calculated with the Cauchy formula $n = A + B\lambda^{-2}$ (λ is the light wavelength), using for keratin $A_k = 1.532$ and $B_k = 5890 \text{ nm}^{-2}$ and for melanin $A_m = 1.648$ and $B_m = 23700 \text{ nm}^{-2}$; the imaginary component of the refractive index of keratin was assumed to be negligible in the wavelength range of interest, but that of melanin was taken to be $k_m = a_m \exp(-\lambda/b_m)$, with $a_m = 0.56$ and $b_m = 270 \text{ nm}$ [10,13]. The effective refractive index of each 1 nm layer was calculated with the volume fractions of the components:

$$n_{\text{eff}} = (f_k n_k^w + f_m n_m^w)^{1/w}. \quad (2.1)$$

Effective medium theory predicts for TE- and TM-polarized light incident on parallel rods weighting factors: $w = -2$ and 2 [22,23]. We found that w -values between -2 and $+2$ yielded virtually identical reflectance spectra, and therefore we used in the final calculations $w = 1$. We compared the results with calculations performed with Lumerical FDTD solutions 8.16, a commercial-grade Maxwell equation solver. Being based on fundamental Maxwell theory, FDTD simulations enable the detailed simulation of the light flux in any complex-structured material with arbitrary refractive index and spatial arrangement. With the same parameters as those used in the multilayer modelling, simulations were performed in a simulation box with a volume of approximately $3 \times 3 \times 5 \mu\text{m}^3$.

2.7. Photoreceptor sensitivity spectra

Mallards have four main photoreceptors: VS (violet-sensitive), SWS (short-wavelength-sensitive), MWS (middle-wavelength-sensitive) and LWS (long-wavelength-sensitive) [23,24]. The absorption spectra of the photoreceptors can be calculated with the absorption spectra of the visual pigments and their density in the outer segments. The absorption spectra were obtained with the peak wavelength of the visual pigments, 415, 452, 506 and 567 nm, and peak density of the photoreceptors 0.3, using a template [24–26]. In front of the SWS, MWS and LWS photoreceptors oil droplets are located that contain a high concentration of various carotenoids and thus act as spectral

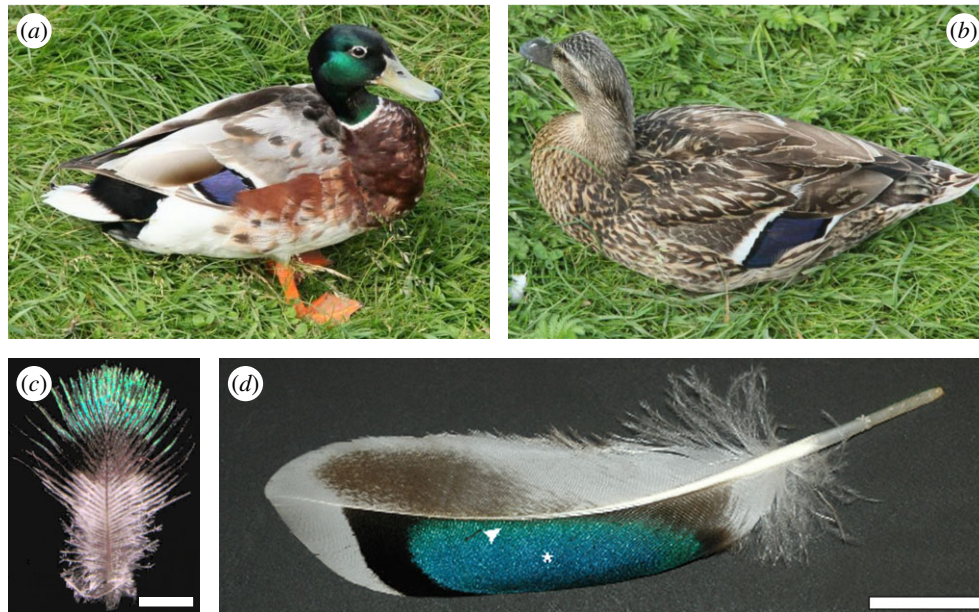


Figure 1. Sexual dichromatism of the mallard, *Anas platyrhynchos*. (a) A drake (male) with a green head and a blue iridescent speculum. (b) A hen (or duck, female) with only the speculum being iridescent. (c) A male head feather. (d) A speculum feather; the asterisk and arrowhead indicate the areas of figure 2*a,b*, respectively. Scale bars: (c) 2 mm, (d) 2 cm.

filters. Hart & Vorobyev [25] approximated the transmittance of the oil droplets with the expression

$$T(\lambda) = \exp[-\exp(-b(\lambda - \lambda_0))], \quad (2.2)$$

and assessed for the SWS, MWS and LWS oil droplets $b = 0.098$, 0.090 and 0.061 , respectively, and $\lambda_0 = 457$, 519 and 580 nm. The transmittance spectra obtained with equation (2.2) can be well understood by assuming in the three oil droplets the carotenoids galloxanthin, zeaxanthin and astaxanthin, respectively, with peak density 5, 20 and 25 [5]. Furthermore, incident light is filtered by the ocular media in front of the retina. The absorption spectrum of the ocular media (fig. 5 in [26]) converted to the transmittance spectrum, normalized and fitted by equation (2.2) yielded $b = 0.064$ and $\lambda_0 = 364$ nm. The spectral filters cause strongly narrowed absorption bands of the photoreceptors. Normalizing the resulting absorption spectra yielded the sensitivity spectra of the four photoreceptors.

3. Results

3.1. Colours and anatomy of head and speculum feathers

The common mallard, *Anas platyrhynchos*, is well known for its sexual dichromatism. The head of the male is marked by a prominent green sheen, highly contrasting with the white and orange-brownish coloration of the body (figure 1*a*). The female has an overall brown colour (figure 1*b*). The only colour correspondence of the two sexes, most notable during flight, is the blue colour of the speculum. The head and speculum colours are iridescent, i.e. the hue varies upon a change in direction of the illumination or inspection.

The head and speculum feathers not only differ in colour, but also strongly in size and organization. In the approximate 1 cm long head feathers of the male (figure 1*c*), only the distal part is structurally coloured. Interestingly, the proximal part is rather colourless, because it is overlapped by adjacent feathers *in situ* (figure 1*a,c*). The overlap extends to the

black middle part of the head feather, which has a contrast-enhancing function for the exposed distal part that displays the green colour. Somewhat differently, the approximate 10 cm long speculum feathers overlap sideways, but again only the exposed feather part is coloured (figure 1*a,b,d*). The distal and proximal boundaries of the displayed sides of adjacent feathers together create highly contrasting black and white bands of the speculum (figure 1*a,b*).

Inspection with a light microscope shows that the iridescence originates in the barbules (figure 2*a,b*). The barbules are coloured at only one side of the barb (figure 2*c,d*). The barbules consist of long rows of brightly coloured individual cells, each with an area approximately $20 \times 30 \mu\text{m}^2$ (figure 2*e-g*). The colour of the cells slightly varies across the speculum, and the colour appears to be not uniform even locally within a single cell (figure 2*a-f*). Interestingly, when observing an isolated barbule from both the upper- and undersides, a similar colour is seen (figure 2*c-f*). Notably, however, the underside of the cells features a pale centre, indicating the remnant of a cell nucleus [13,14,27]. The colours dramatically differ when observed with transmitted light. The barbules then appear to be heavily brown-black pigmented, clearly indicating the presence of melanin pigment (figure 2*g*).

TEM demonstrates that the melanin of the barbule cells is concentrated in rod-like structures, the so-called melanosomes [6,7], that are oriented along the barbule's longitudinal axis (figure 3*a*), causing the striped pattern seen with transmission light microscopy (figure 2*g*). Cross sections show a highly symmetric pattern where a cortex, with thickness approximately 270 nm, envelopes two stacks of melanosomes, tightly packed into a lattice of five to six rows, with in-between randomly arranged melanosomes (figure 3*b*). The size of the individual melanosomes somewhat varies; in the specific case of figure 3*c*, the length is $1.5\text{--}2.0 \mu\text{m}$ and the diameter approximately 130 nm. The spatial arrangement is also somewhat irregular, clearly deviating from an ideal hexagonal stacking, especially at the side of the stacks facing the barbule's axis.

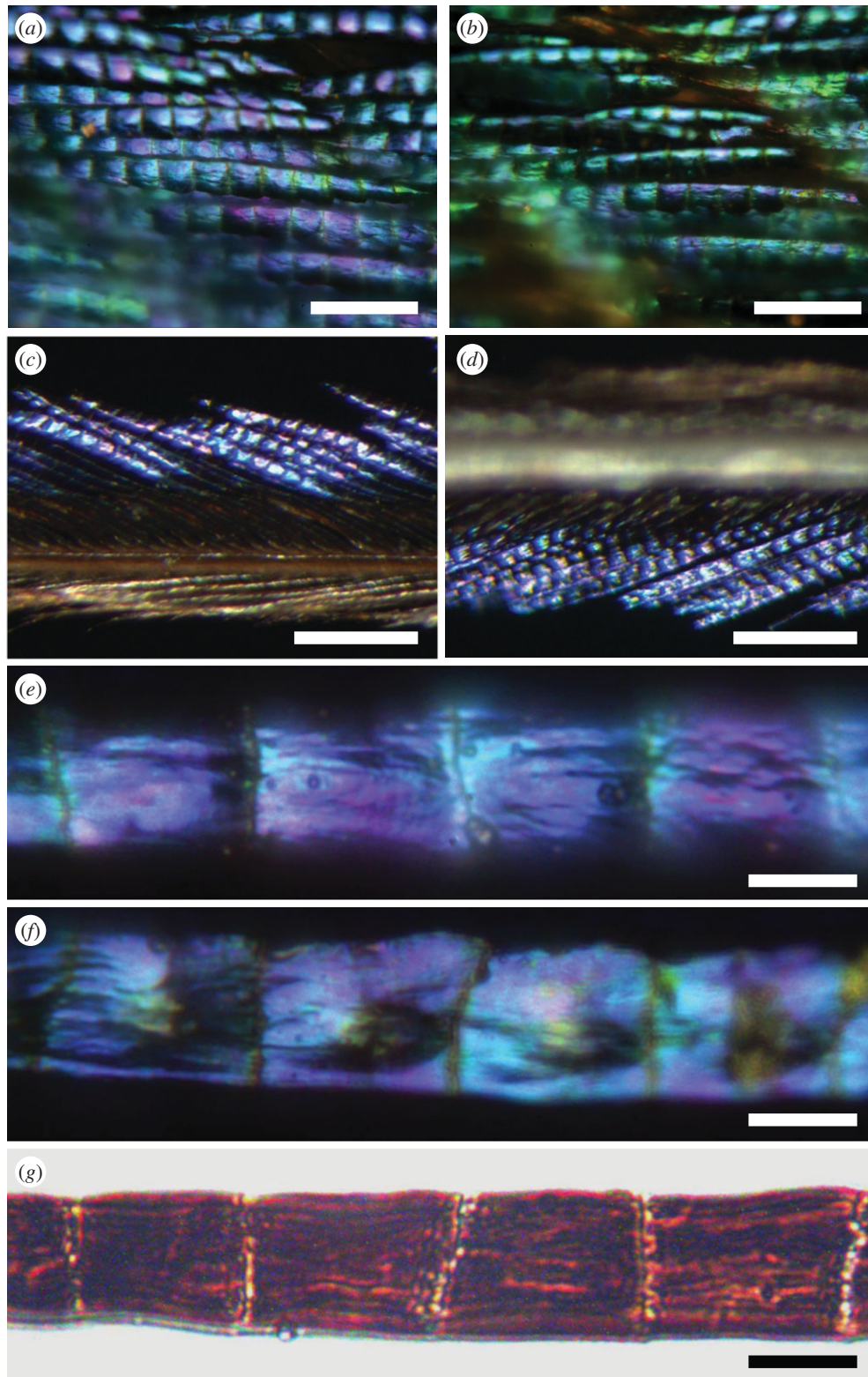


Figure 2. Light microscopy of speculum feather barbules. (a) Closely packed barbules in a central area of the blue iridescent area of the intact feather (asterisk in figure 1*d*). (b) Greenish-iridescent area near the rachis (arrowhead in figure 1*d*). (c) Upperside of a speculum barb with asymmetrically coloured barbules. (d) Underside of the speculum barb. (e) Epi-illumination light micrograph of the upperside of an isolated barbule. (f) The underside of the same barbule with epi-illumination. (g) Transmitted light micrograph of the same barbule. Scale bars: (a,b) 100 μm , (c,d) 200 μm , (e–g) 20 μm .

3.2. Spectrometry and imaging scatterometry reveal multilayer characteristics

Interference of incident light with the lattice of melanosomes must cause the barbule's colours, and we therefore performed spectrometry as well as imaging scatterometry. Reflectance spectra measured by MSP from the upper and undersides of single barbule cells of speculum and head

feathers yielded narrow-band spectra (FWHM 70–90 nm) with peak wavelengths at approximately 470 nm (figure 4*a*) and approximately 540 nm (figure 4*b*). Depending on the location, the spectra slightly varied in magnitude and spectral position (see the varying colours in figure 2*e,f*). Interestingly, the rising long-wavelength tail showed small but characteristic oscillations. These can be readily explained from the thickness of the barbule cells, 4–5 μm (figure 3*a,b*),

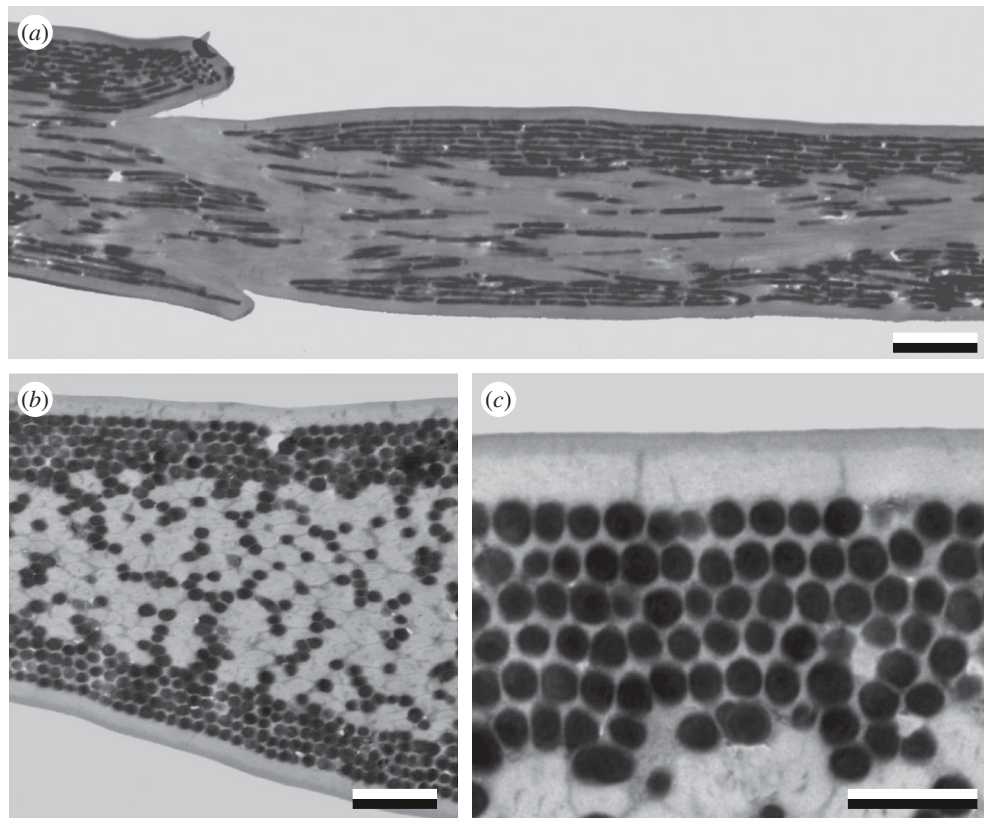


Figure 3. TEM images of a speculum barbule. (a) Longitudinal section showing the transition area of two cells. (b) Cross section showing melanosome stacks near both the upper- and undersides of the barbule. (c) Higher magnification showing the slightly irregular packing and the varying size of the melanosomes. Scale bars: (a) 2 μm , (b) 1 μm , (c) 0.5 μm .

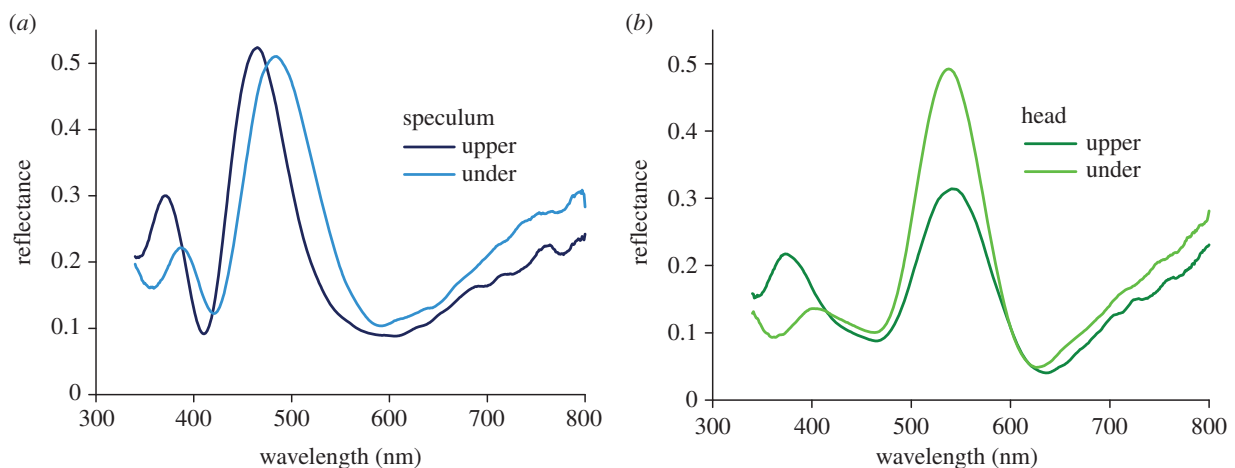


Figure 4. Reflectance spectra of mallard feather barbules. (a) Spectra of an isolated speculum barbule measured from the upper- and undersides of the same cell with a MSP. (b) MSP spectra from the upper- and undersides of the same cell of a head feather barbule.

when assuming an effective refractive index of approximately 1.6 [28]; for examples with more prominent oscillations, see the electronic supplementary material, figure S1.

To quantitatively investigate the iridescence, we measured the reflectance of a speculum feather (figure 1*d*) as a function of polarization and angle of light incidence (figure 5*a,b*). In the measurements of figure 5*a,b*, the detection angle was changed mirror-wise; that is, the angle between the detector and the normal to the feather plane was equal but opposite the angle between the illumination and the normal. The reflectance peak wavelengths, derived from the spectra of figure 5*a,b*, decreased monotonically with increasing angle of light incidence for both TE- and TM-polarized light (figure 5*c*). Although the value of the peak reflectance of the TE-reflectance increased with increasing incidence angle, the TM-reflectance

decreased up to an angle of incidence of approximately 60° and increased above that value (figure 5*d*).

The angle dependence of the reflectance spectra of the TE- and TM-polarizations is characteristic for a multilayer structure [28,29]. The assembly of barbules in the mallard feathers may, however, not function as an ideal, classical optical multilayer, because that acts as a mirror, i.e. it reflects light from a point source into the mirror angle. To see to which extent the individual barbule cells approximate an ideal multilayer, we tested the spatial reflection properties of barbules of both speculum and head feathers using an imaging scatterometer (figure 6). In both cases, focusing a white light beam with aperture approximately 5° at a barbule cell with spot size approximately $13 \mu\text{m}$ caused a reflected beam with a slightly widened aperture of approximately 20°

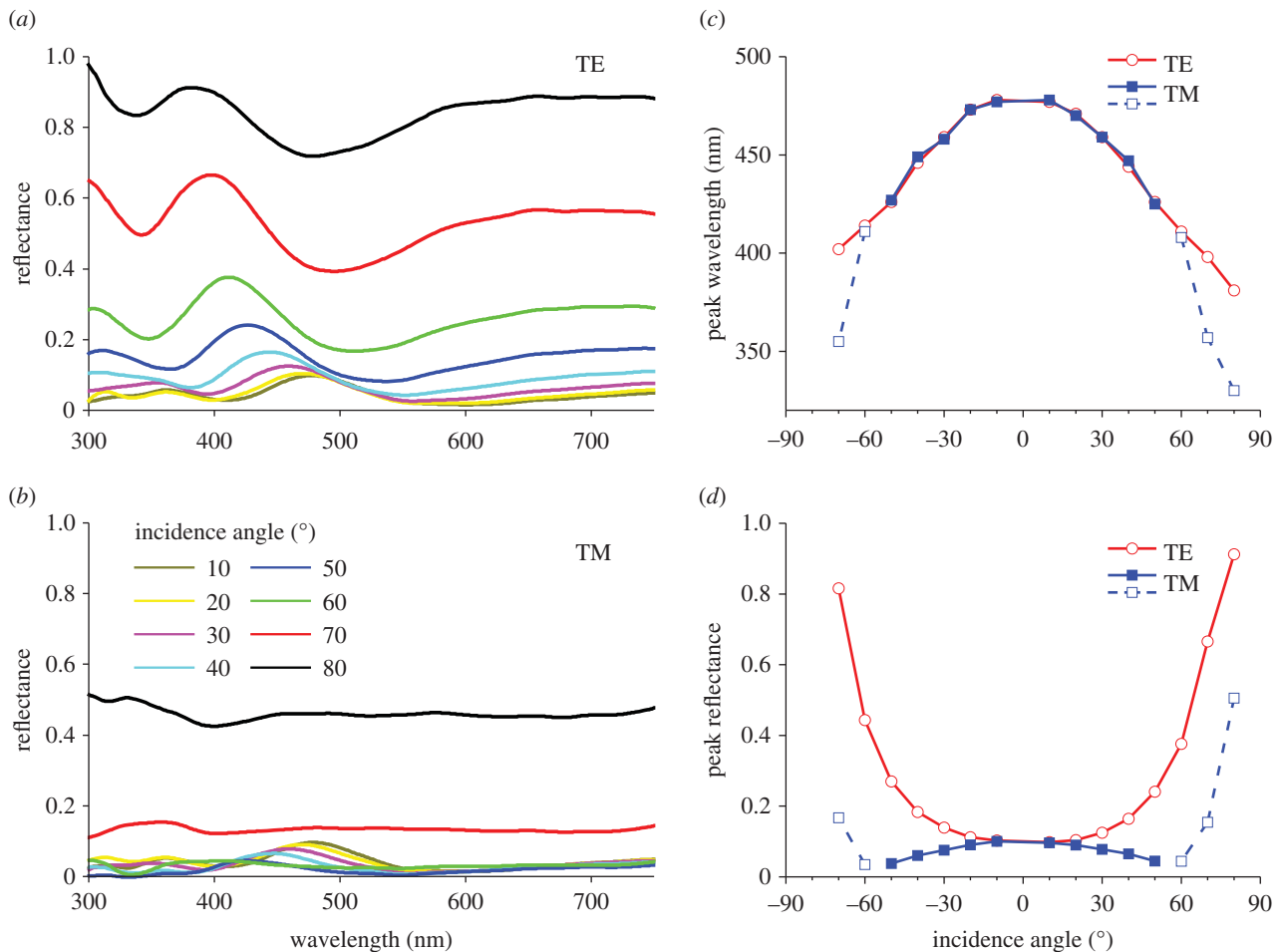


Figure 5. Angle dependence of mallard speculum feather reflections. (a) Reflectance spectra measured with TE-polarized light while changing the angle of light incidence in steps of 10° and the angle of the detector mirror-wise. (b) Reflectance spectra measured with TM-polarized light. (c) Peak wavelengths of the reflectance spectra of (a,b). (d) Peak reflectance values of the spectra of (a,b). The open symbols and dashed lines for TM-polarized light in (c) and (d) indicate that the peak values are not fully adequate, due to the phase reversal that occurs above Brewster's angle.

(figure 6a,b). The minor spread of the barbule reflection can be easily understood from the non-planar, inhomogeneous arrangement of the melanosomes when considering areas larger than a few micrometres (figure 3a). Applying light with a 90° aperture beam shows clear radial-symmetric iridescence (figure 6c,d), reinforcing the view that the reflection properties of single barbules can be locally interpreted with multilayer theory.

3.3. Multilayer and finite-difference time-domain modelling of mallard barbules

We computationally investigated the reflection characteristics of the melanosomes stacks in the barbules with a multilayer model (figure 7a, inset). In the model, a keratin layer, thickness t_b , contains two stacks of m layers of melanosomes, with melanosome axial interdistance a , layer period b , melanosome diameter d_m . The two stacks are separated by an interdistance t_i and enveloped by a cortex with thickness c . Based on the anatomy, we chose as initial model values $m = 6$, $a = 145$ nm, $b = 160$ nm, $c = 270$ nm, $d_m = 130$ nm, $t_i = 2000$ nm, yielding $t_b = 4400$ nm; subsequently, in more detailed modelling, we varied these values.

As described in the Material and methods, we sliced the model of figure 7a in 1 nm thin layers and calculated for each layer the fraction of keratin and melanin, yielding with equation (2.1) the complex refractive index as a function of wavelength. With the obtained wavelength-dependent

refractive index profile, we calculated the reflectance spectrum of the model barbule for normally incident light using a transfer-matrix method. To ascertain the validity of the multilayer approach, we also used the FDTD method to calculate the reflectance spectrum of a full three-dimensional model for normally incident light, which for TE- and TM-polarized light yielded only slightly different spectra (figure 7b). Satisfactorily, the FDTD spectra were almost identical to those resulting from the multilayer calculations.

The calculated reflectance spectra showed high-frequency oscillations, especially in the longer wavelength range and also in the main reflectance band near 500 nm, presumably due to interference of light reflected at both surfaces of the model barbule that acts as a thin film. We therefore calculated the reflectance spectra for varying thicknesses t_i of the intermediate keratin layer of the model barbule, which yielded spectra with shifted oscillations (electronic supplementary material, figure S2a). Real barbules deviate from the model in that the upper and under surfaces are not at all perfectly parallel (figure 3a,b). We therefore performed model calculations keeping the cortex and melanosome stacks constant, but assuming a Gaussian distribution of the intermediate keratin layer thickness, with standard deviation σ and average $t_i = 2000$ nm. With increasing σ the high-frequency oscillations rapidly decreased, vanishing at $\sigma = 250$ nm (electronic supplementary material, figure S2b). A prominent blue-green reflectance band with only some lower frequency waves then remained (shown in figure 7b,c, $\sigma = 250$ nm).

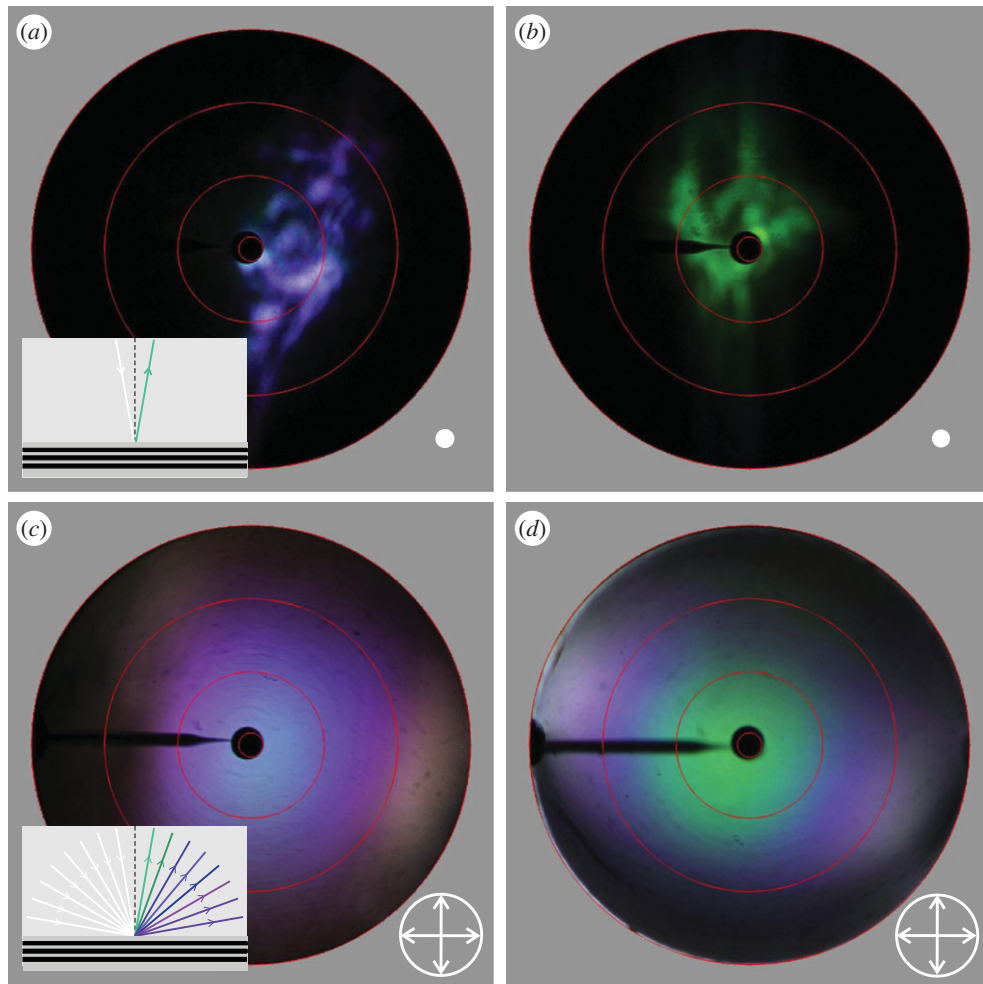


Figure 6. Imaging scatterometry applying white light illumination. (*a,c*) Scatterograms of a barbule cell of a speculum feather. (*b,d*) Scatterograms of a barbule cell of a male head feather. (*a,b*) Illumination with a narrow-aperture beam (indicated by the white dot). (*c,d*) Illumination with a wide-aperture beam of unpolarized light (indicated by arrowed horizontal and vertical lines in a circle). Insets: the barbule reflects light specularly (*a*), which results in iridescence when illumination is applied from various angles (*c*). The red circles indicate angles of 5°, 30°, 60° and 90°; the black, pointed rod at 9 o'clock is the shade created by the glass pipette carrying the feather barbule, and the central black spot is due to the central hole of the scatterometer's ellipsoidal mirror allowing axial illumination with a narrow-aperture beam.

To investigate the relative importance of the two stacks of melanosomes, we calculated the reflectance and transmittance spectra for only the distal half of the barbule, i.e. with only the distal cortex, one melanosome stack and a keratin medium ending at a distance $t_b/2$ from the surface (indicated by the dashed vertical line in figure 7*a*). The spectra obtained with the transfer-matrix and FDTD calculations were again virtually identical; of course, the spectrum of the half barbule showed no high-frequency oscillations because the last layer was keratin and not air (figure 7*c*). The main green bands in the reflectance spectra of the Gaussian-varied full barbule ($\sigma = 250$ nm) and the half barbule appeared to be almost identical. The spectra slightly deviate at the longer wavelengths, where the full barbule's reflectance is somewhat higher than that of the half barbule (figure 7*c*). This is understandable from the decreasing absorption, or increasing transparency, of the melanosome stacks with increasing wavelength as illustrated by the transmittance spectra of figure 7*d*. The transmittance calculated for only one melanosome stack is greater than 0.5 at wavelengths above 600 nm (figure 7*d*, half), so that in the full barbule the second melanosome stack contributes to the total reflectance in the long-wavelength range (figure 7*c*).

The transmittance spectra calculated for the full barbule with the transfer-matrix and FDTD methods are similar (figure 7*d*), but they are still substantially higher than the spectrum measured from an immersed barbule by MSP (figure 7*d*). The latter can be understood from the fact that in the calculations the keratin layer between the melanosome stacks was assumed to be fully made up of keratin, i.e. to be transparent. The considerable number of randomly arranged melanosomes in the inner medium, between the two melanosome stacks (figure 3), will add substantially to absorption, and hence reduce the transmittance.

Varying the thickness of the intermediate keratin layer while keeping the other parameters fixed caused smoothing of the fine-structured reflectance spectrum of the model barbule (figure 7*b* and electronic supplementary material, figure S2). Similar effects can be expected in barbules where the other parameters vary. We investigated this by calculating the reflectance spectra of the half barbule of figure 7*c* for different parameter values. First, we calculated reflectance spectra for various values of the number of melanosome layers, m . An increase in m causes an obvious increase in peak reflectance, and furthermore the bandwidth slightly narrows and a small bathochromic (towards longer wavelengths) peak

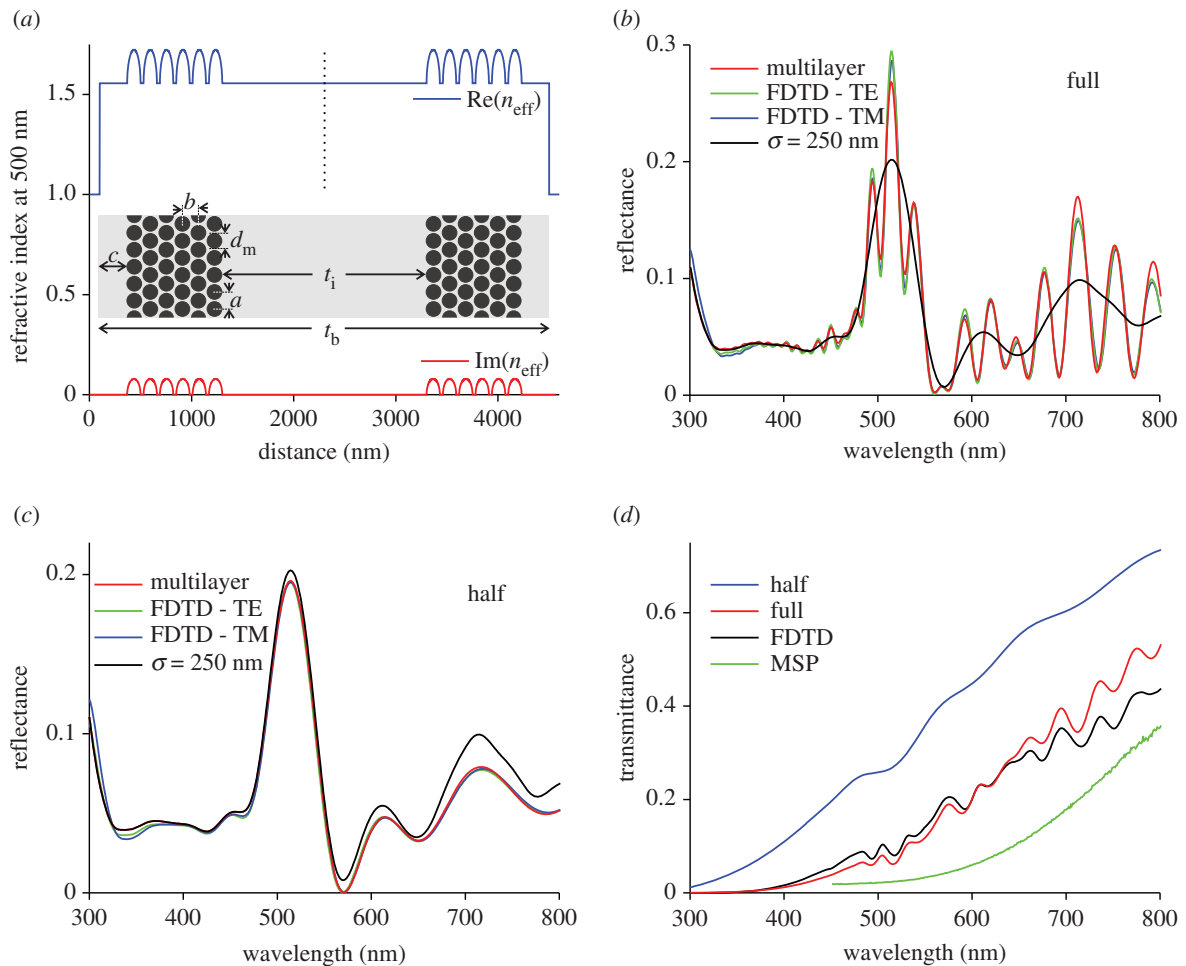


Figure 7. Modelling the reflectance of mallard barbules. (a) Real and imaginary parts of the effective refractive index at 500 nm, $\text{Re}(n_{\text{eff}})$ and $\text{Im}(n_{\text{eff}})$, respectively, of the model barbule shown as inset, with lateral distance of the melanosomes a , layer distance b , cortex thickness c , melanosome diameter d_m , thickness of intermediate keratin layer t_i and full barbule thickness t_b . The dashed vertical line indicates the barbule's symmetry plane. (b) Reflectance spectra for normally incident light calculated with the multilayer and FDTD methods for the full model barbule of (a), and the reflectance spectrum for a barbule with a Gaussian varying intermediate keratin layer thickness with standard deviation $\sigma = 250$ nm. (c) Reflectance spectra calculated with the multilayer and FDTD methods for the distal half of the barbule, and the reflectance spectrum of (b) for a full barbule with a Gaussian varying intermediate layer thickness with standard deviation $\sigma = 250$ nm. (d) Transmittance spectra of the half and full barbule calculated with the multilayer approach and of the full barbule calculated with the FDTD method, compared with a spectrum measured with an MSP.

shift occurs (figure 8a). The latter results from the combined cortex and melanosome stack, as may be concluded from the increase in the frequency of the waves in the greater than 600 nm spectral range with increasing layer number. Anatomy shows that the layer number varies (figure 3), and the shift in the spectral waves of figure 8a hence explains that the reflectance spectra will be smoothed and that as a consequence the experimental spectra of figure 4 do not feature the waviness in the higher spectral range.

Increasing the value of the spacing of the melanosomes in the layers, a , causes both a decrease in peak reflectance and a slight hypsochromic (towards shorter wavelengths) shift of the reflectance spectra, due to the decrease in the effective refractive index of the melanosome layers (figure 8b). An increase in the multilayer period, b , results in a bathochromic shift of the reflectance peak (figure 8c). This behaviour can be interpreted with the rule $\lambda_{\text{max}} = 2(n_1d_1 + n_2d_2)$ for a multilayer built up of two components with refractive indices n_1 and n_2 and thicknesses d_1 and d_2 . As an example, taking $n_1 = 1.55$ and $n_2 = 1.65$ and $b/2 = d_1 = d_2 = 80$ nm, yields $\lambda_{\text{max}} = 512$ nm. Higher (lower) values will result with an increasing (decreasing) multilayer period. We must emphasize, however, that light interference in the combined

structure consisting of the upper thin-film cortex and the multilayer stack ultimately determines the reflectance spectrum. The importance of the cortex is shown by figure 8d, where an increasing cortex thickness, c , causes an increase in both the peak reflectance and peak wavelength.

The measurements yielded a reflectance peak wavelength for the blue speculum of approximately 470 nm and for the green head of approximately 540 nm. The treated model yielded a peak wavelength of 510 nm for a multilayer period 160 nm and cortex thickness 270 nm. We found that the peak wavelength is most sensitive for changes in the multilayer period and cortex thickness, and therefore presumably the speculum feather barbule's period and cortex thickness are smaller than the model values, approximately 140 and approximately 250 nm (figure 8e), and the values of the green head barbules are larger, approximately 170 nm and approximately 280 nm (figure 8f). Figure 8e shows reflectance spectra obtained for a half barbule with the initial parameter values except that $b = 140$ nm and $c = 250$ nm while the number of melanosome layers was $m = 5, 6$ and 7, respectively. The averaged spectrum has a peak wavelength at $\lambda_{\text{max}} = 468$ nm, approximately that of a speculum barbule; note that averaging removes the waviness of the

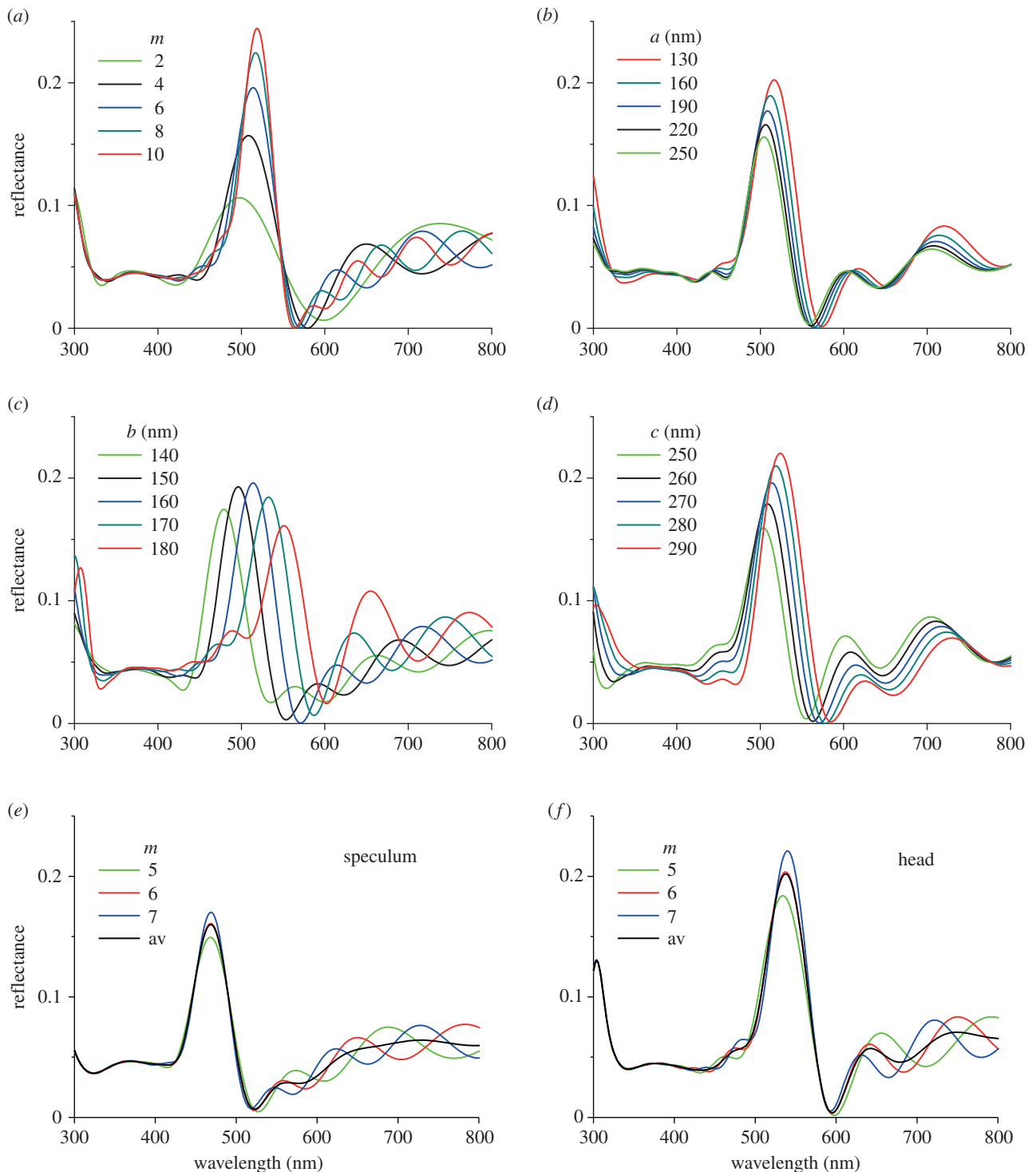


Figure 8. Dependence of barbule reflectance on melanosome parameters (normally incident light) calculated with the transfer-matrix procedure for the distal half of the barbule. (a–d) The effect of varying the number of melanosome layers, m , the lateral period of melanosomes, a , the multilayer period, b , and the cortex thickness, c . The initial parameter value set was $m = 6$, $a = 145$ nm, $b = 160$ nm, $c = 270$ nm, with diameter of the melanosomes $d_m = 130$ nm. (e) Modelling the speculum feather reflectance with $b = 140$ nm and $c = 250$ nm. (f) Modelling the head feather reflectance with $b = 170$ nm and $c = 280$ nm. In (e,f), av indicates the average of the spectra obtained with $m = 5, 6$ and 7.

spectrum in the longer wavelength range (figure 8e, av). Similarly, figure 8f shows reflectance spectra for $b = 170$ nm and $c = 280$ nm for $m = 5, 6$ and 7. The peak wavelength of the averaged spectrum is $\lambda_{\max} = 538$ nm, approximately that of a head feather barbule. (For a direct comparison of the reflectance spectra of figure 8e,f and the experimental spectra of figure 4, see the electronic supplementary material, figure S3.) Minor changes in the parameter values hence result in substantial colour changes. The light micrographs and anatomy of figures 2 and 3 indeed show that the

parameter values are not constant. This means that light interference in melanosome stacks of barbules with varying parameters will yield smoothed reflectance spectra. We have investigated this further below.

3.4. Consequences of disorder in the melanosome arrangement

In the above modelling, we assumed a perfectly ordered arrangement of identically sized melanosomes inside the

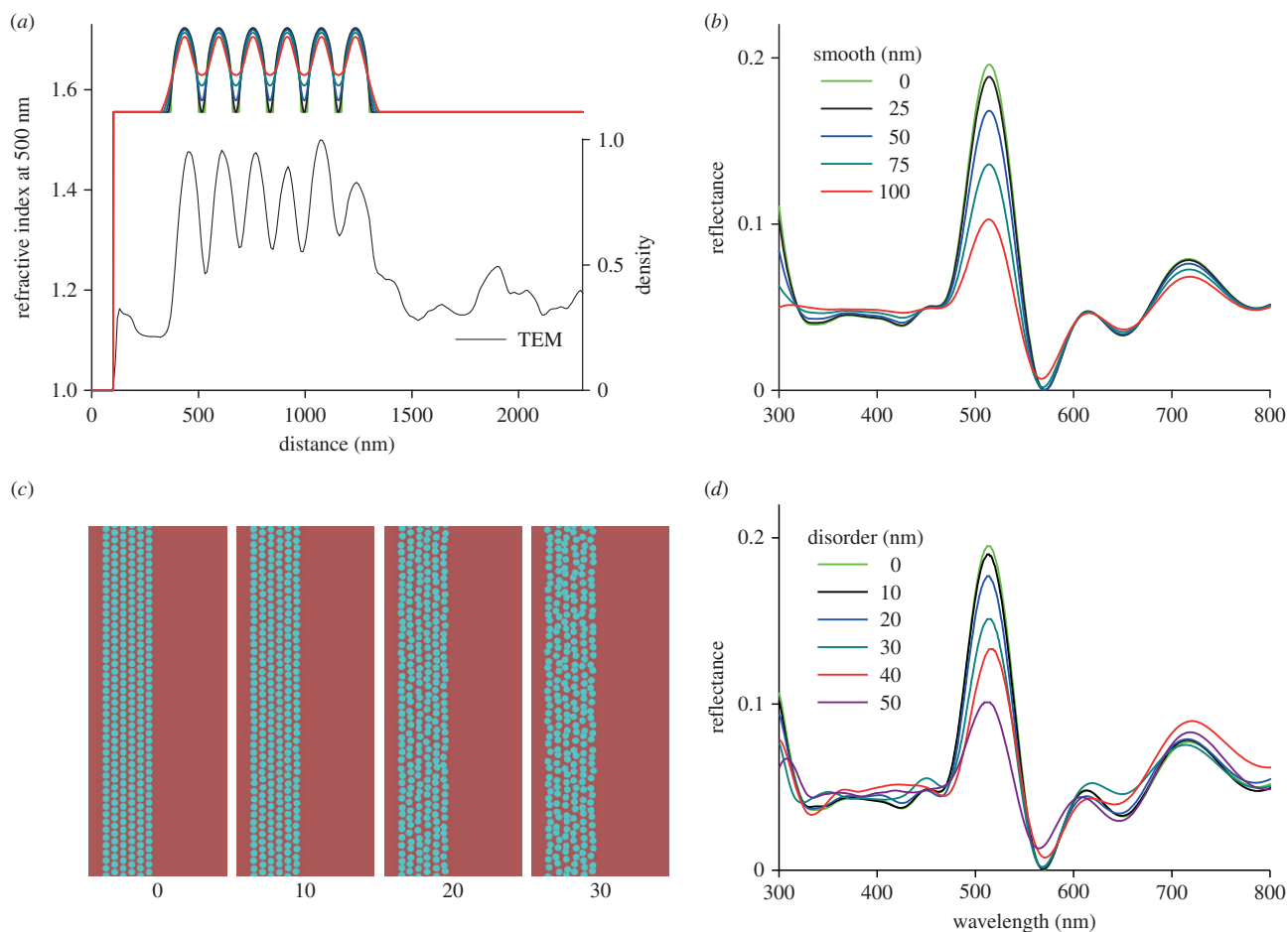


Figure 9. Disorder in the melanosome arrangement. (a) The refractive index (real part) profile of half the model barbule of figure 7a, smoothed with smoothing windows 0, 25, 50, 75 and 100 nm (see (b)), and the normalized averaged density profile of a 2000 nm wide section perpendicular to the cortex surface of a TEM image (figure 3c). (b) Reflectance spectra calculated with the transfer-matrix method using the various smoothed refractive index profiles of (a). (c) Diagrams showing six layers of melanosomes with perfect order (0), and with various degrees of disorder (10–30, see (d)). (d) Reflectance spectra calculated with the FDTD method for the various disordered melanosome arrangements. The given disorder values are the averages of the random spatial displacements.

barbules, but our anatomical results showed that the melanosomes are only roughly orderly arranged and also vary somewhat in size. We studied the effect of melanosome disorder in two ways. We first smoothed the refractive index profile of figure 7a to various degrees, resulting in a more or less sinusoidal depth dependence, well corresponding to the density profiles following from transmission electron micrographs (figure 9a). The reflectance spectra calculated with the transfer-matrix method show that an increase in the smoothing window, resulting in a decreasing refractive index contrast, causes a decrease in the peak amplitude (figure 9b).

We also performed FDTD calculations for half barbules with disordered melanosome stacks (figure 9c). The melanosome position was varied randomly with a maximal displacement of 10–50 nm, resulting in spectra with gradually decreasing amplitude (figure 9d), very similar as found with the smoothed refractive index profile and the transfer-matrix approach (figure 9b). The spectra calculated for the smoothed multilayer profiles have all the same peak wavelength, because the multilayer period stays constant with smoothing, but the FDTD spectra of figure 9d show a slight variation in peak wavelength, which is due to disorder-induced change in the multilayer period. In summary, the close correspondence of the multilayer and FDTD calculations for disordered melanosomes corroborates the

findings above that the barbule photonics is well approximated by multilayer optics.

This conclusion was further confirmed by calculating the reflectance spectra as a function of the angle of incidence, for both TE- and TM-polarized light, for (half) the model barbule of figure 7. Transfer-matrix as well as FDTD calculations yielded again virtually identical results (electronic supplementary material, figure S4). Furthermore, the angle dependence of the peak wavelength and peak reflectance corresponded closely with those of the experimental spectra of figure 5.

3.5. Tuning of feather reflectance spectra to photoreceptor sensitivity spectra

The colours of the speculum and head feathers as seen by human eyes are very different. That the barbule's reflectance spectra are indeed well separated (figure 4) indicates a distinct difference in the spacing of the melanosome layers, the principal parameter that determines the spectral location of the reflectance band (figure 8c). Presumably, the feather colours are also quite different for the mallard visual system, and we therefore compared the reflectance spectra with the spectral sensitivities of the photoreceptors of mallards (figure 10). We calculated the photoreceptor spectral sensitivities as described in the Material and methods (figure 10, dashed curves), yielding as peak wavelengths of the four

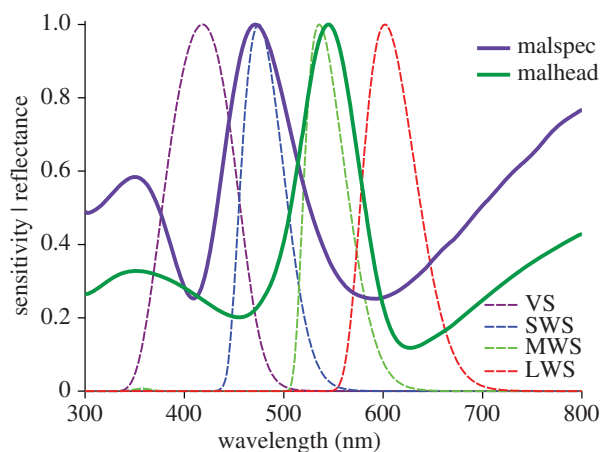


Figure 10. Duck structural colours and photoreceptor spectral sensitivities. Normalized reflectance spectra of the mallard speculum (malspec) and head feathers (malhead) measured with a bifurcated reflection probe. The sensitivity spectra of the VS, SWS, MWS and LWS photoreceptors were calculated as described in the Material and methods.

photoreceptor types (VS, SWS, MWS and LWS) 418, 475, 536 and 604 nm, respectively. The reflectance spectra of the mallard speculum and head feathers measured with a bifurcated probe, with peak wavelengths 472 and 545 nm, closely correspond to the sensitivity spectra of the SWS and MWS cone photoreceptors (figure 10). The close correspondence of the feather reflectance spectra with the photoreceptor spectral sensitivities suggests spectral tuning of the duck feathers to the characteristics of the visual system.

4. Discussion

The structural colours of mallard barbules can be almost fully attributed to the stack of melanosomes at the side exposed to the incident light, because the contribution of the other stack appears to be very minor (figure 7c). The lower stack is about equally well reflecting, and our anatomical investigations show that the two stacks have a very similar organization (figure 3). Presumably, the cellular processes responsible for concentrating the melanosomes into stacks during development favour a symmetrical assembly of the melanosomes [30]. The second stack still has a useful optical function by acting as a straylight absorber.

Calculations for perfectly arranged and imperfect stacks yielded very similar reflectance spectra even at high levels of spatial disorder (figure 9), demonstrating that the coloration created by the melanosome stacks is surprisingly robust to irregularities in the melanosome arrangement (as well as size disorder; see the electronic supplementary material, figure S5). The virtual identity of the spectra resulting from the transfer-matrix method and the FDTD modelling proved that the melanosome stacks can indeed be successfully treated as multilayers. This is in full agreement with the view expounded decades ago by Durrer [9]. Recently, this view has been challenged by claiming that the arrangement of the melanosomes in a hexagonal lattice creates a two-dimensional photonic crystal, which together with the thin-film cortex forms a photonic heterostructure [16]. However, the cortex and melanosome stack act together as an integrated optical system. One of the bands in the reflectance spectrum cannot be therefore claimed to be due to only the thin-film cortex [16]. The analysis presented here

demonstrated that treating the melanosome stack together with the cortex as a multilayer allows a detailed optical description of the barbules, so providing an in-depth insight into the spectral consequences of the various dimensional parameters for both the angle and polarization dependence. We note that our model presented in figures 7–9 generally applies to iridescent mallard feathers. Owing to the scale invariance of the Maxwell equations, a different size of the melanosomes results in direct scaling of the reflectance band [16]. In other words, smaller/larger melanosomes with a smaller/larger interdistance will have a blue- or red-shifted optical response, respectively.

The melanosomes are longitudinal rods, closely packed and arranged parallel to each other along the barbule axis (figure 3). This arrangement together with the higher refractive index of melanin with respect to that of the surrounding keratin causes anisotropy [16]. In the latter paper and other past literature, the refractive index of melanin was assumed to be 2.0, however, without proper experimental evidence. In direct measurements on feather barbules of the bird of paradise *Parotia lawesii*, we recently found that the refractive index of melanin is significantly lower, being approximately 1.8 at 400 nm, gradually declining to approximately 1.7 at 700 nm [13]. Accordingly, the refractive index difference of melanin and keratin is rather moderate (0.15–0.20 [8,11]), and thus the difference between the resulting effective refractive indices for light polarized parallel and perpendicular to the barbule axis remains very small. Indeed, multilayer modelling using anisotropy-corrected refractive index values (equation (2.1)) yielded only very slightly different reflectance spectra. The reflectance spectra obtained in the FDTD calculations were also virtually identical for TE- and TM-polarized light (figure 7b and electronic supplementary material, figure S4). Given the ample existence of varying parameter values causing distinct changes in the reflectance spectra, we therefore conclude that anisotropy can be easily neglected in the present case of the barbules of mallards.

The peak wavelengths of the reflectance spectra of the mallard's blue speculum and green head feathers approximate the peak wavelengths of the SWS and MWS photoreceptor cells. Although the bandwidths of the reflectance spectra are distinctly wider than the bandwidths of the photoreceptor sensitivity spectra, the co-localized spectra strongly suggest that the feather spectra are tuned to the photoreceptor spectra. Similar correspondences of feather and photoreceptor spectra were found to exist in other birds, e.g. parrots, where the feathers are coloured by both structural and pigmentary effects [31] and passerines, which feature purely pigmentary coloration [5,32]. As bird photoreceptors have a remarkably small variation in the spectral distribution of their photoreceptor sensitivities [25], this creates an excellent case for further studies on the evolution of bird coloration.

Data accessibility. All data needed to evaluate the conclusions in the paper are present in the paper and/or the electronic supplementary material. Additional data related to this paper may be requested from the authors.

Authors' contributions. Multilayer modelling was performed by D.G.S., FDTD modelling by B.D.W. All authors performed experiments and participated in writing the manuscript.

Competing interests. We declare we have no competing interests.

Funding. This study was financially supported by the Air Force Office of Scientific Research/European Office of Aerospace Research and

Development AFOSR/EOARD (grant no. FA9550-15-1-0068, to D.G.S.), the National Centre of Competence in Research 'Bio-Inspired Materials' and the Ambizione program of the Swiss National Science Foundation (168223, to B.D.W.).

Acknowledgements. We thank Dr Julian Thorpe (University of Sussex, UK) for performing TEM and Dr Daniel Osorio for advice and reading the manuscript. Three anonymous referees provided valuable, constructive criticisms.

References

1. Fox HM, Vevers G. 1960 *The nature of animal colours*. London, UK: Sidgwick and Jackson.
2. Hill GE, McGraw KJ. 2006 *Bird coloration, vol. 1: mechanisms and measurements*. Cambridge, MA: Harvard University Press.
3. Kinoshita S. 2008 *Structural colors in the realm of nature*. Singapore: World Scientific.
4. McGraw KJ. 2006 Mechanics of carotenoid-based coloration. In *Bird coloration*, vol. 1 (eds GE Hill, KJ McGraw), pp. 177–242. Cambridge, MA: Harvard University Press.
5. Stavenga DG, Wilts BD. 2014 Oil droplets of bird eyes: microlenses acting as spectral filters. *Phil. Trans. R. Soc. B* **369**, 20130041. (doi:10.1098/rstb.2013.0041)
6. McGraw KJ. 2006 Mechanics of melanin-based coloration. In *Bird coloration*, vol. 1 (eds GE Hill, KJ McGraw), pp. 243–294. Cambridge, MA: Harvard University Press.
7. Hill GE. 2010 *Bird coloration*. Washington, DC: National Geographic.
8. Prum RO. 2006 Anatomy, physics, and evolution of avian structural colors. In *Bird coloration*, vol. 1 (eds GE Hill, KJ McGraw), pp. 295–353. Cambridge, MA: Harvard University Press.
9. Durrer, H. 1977 Schillerfarben der Vogelfeder als Evolutionsproblem. *Denkschr. Schweiz. Naturforsch. Ges.* **91**, 1–126.
10. Leertouwer HL, Wilts BD, Stavenga DG. 2011 Refractive index and dispersion of butterfly scale chitin and bird feather keratin measured by interference microscopy. *Opt. Express* **19**, 24 061–24 066. (doi:10.1364/OE.19.024061)
11. Stavenga DG, Leertouwer HL, Wilts BD. 2013 Quantifying the refractive index dispersion of a pigmented biological tissue using Jamin–Lebedeff interference microscopy. *Light Sci. Appl.* **2**, e100. (doi:10.1038/lsa.2013.56)
12. Wilts BD, Michielsen K, DeRaedt H, Stavenga DG. 2014 Sparkling feather reflections of a bird-of-paradise explained by finite-difference time-domain modeling. *Proc. Natl Acad. Sci. USA* **111**, 4363–4368. (doi:10.1073/pnas.1323611111)
13. Stavenga DG, Leertouwer HL, Osorio DC, Wilts BD. 2015 High refractive index of melanin in shiny occipital feathers of a bird of paradise. *Light Sci. Appl.* **4**, e243. (doi:10.1038/lsa.2015.16)
14. Rutschke E. 1966 Die submikroskopische Struktur schillernder Federn von Entenvogeln. *Z. Zellforsch.* **73**, 432–443. (doi:10.1007/BF00329021)
15. Dyck J. 1976 Structural colours. In *Proc. 16th Int. Ornithological Congress* (eds HJ Frith, JH Calaby), pp. 426–437. Canberra, Australia: Australian Academy of Science.
16. Eliason CM, Shawkey MD. 2012 A photonic heterostructure produces diverse iridescent colours in duck wing patches. *J. R. Soc. Interface* **9**, 2279–2289. (doi:10.1098/rsif.2012.0118)
17. Khudiyev T, Dogan T, Bayindir M. 2014 Biomimicry of multifunctional nanostructures in the neck feathers of mallard (*Anas platyrhynchos* L.) drakes. *Sci. Rep.* **4**, 4718. (doi:10.1038/srep04718)
18. Thorpe JR, Tang H, Atherton J, Cairns NJ. 2008 Fine structural analysis of the neuronal inclusions of frontotemporal lobar degeneration with TDP-43 proteinopathy. *J. Neural Transm.* **115**, 1661–1671. (doi:10.1007/s00702-008-0137-1)
19. Stavenga DG, Leertouwer HL, Piriš P, Wehling MF. 2009 Imaging scatterometry of butterfly wing scales. *Opt. Express* **17**, 193–202. (doi:10.1364/OE.17.000193)
20. Wilts BD, Leertouwer HL, Stavenga DG. 2009 Imaging scatterometry and microspectrophotometry of lycaenid butterfly wing scales with perforated multilayers. *J. R. Soc. Interface* **6**, S185–S192. (doi:10.1098/rsif.2008.0299.focus)
21. Vukusic P, Stavenga DG. 2009 Physical methods for investigating structural colours in biological systems. *J. R. Soc. Interface* **6**, S133–S148. (doi:10.1098/rsif.2008.0386.focus)
22. Lucarini V, Saarinen JJ, Peiponen K, Vartiainen EM. 2005 *Kramers-Kronig relations in optical materials research*. Berlin, Germany: Springer.
23. Halir R *et al.* 2015 Waveguide sub-wavelength structures: a review of principles and applications. *Laser Phot. Rev.* **9**, 25–49. (doi:10.1002/lpor.201400083)
24. Govardovskii VI, Fyhrquist N, Reuter T, Kuzmin DG, Donner K. 2000 In search of the visual pigment template. *Vis. Neurosci.* **17**, 509–528. (doi:10.1017/S0952523800174036)
25. Hart NS, Vorobyev M. 2005 Modelling oil droplet absorption spectra and spectral sensitivities of bird cone photoreceptors. *J. Comp. Physiol. A* **191**, 381–392. (doi:10.1007/s00359-004-0595-3)
26. Jane S, Bowmaker J. 1988 Tetrachromatic colour vision in the duck (*Anas platyrhynchos* L.): microspectrophotometry of visual pigments and oil droplets. *J. Comp. Physiol. A* **162**, 225–235. (doi:10.1007/BF00606087)
27. Schmidt WJ. 1952 Wie entstehen die Schillerfarben der Federn? *Naturwissenschaften* **39**, 313–318. (doi:10.1007/BF00589370)
28. Stavenga DG. 2014 Thin film and multilayer optics cause structural colors of many insects and birds. *Mater. Today Proc.* **15**, 109–121. (doi:10.1016/j.matpr.2014.09.007)
29. Yeh P. 2005 *Optical waves in layered media*. Hoboken, NJ: Wiley-Interscience.
30. Shawkey MD, D'Alba L, Xiao M, Schutte M, Buchholz R. 2015 Ontogeny of an iridescent nanostructure composed of hollow melanosomes. *J. Morphol.* **276**, 378–384. (doi:10.1002/jmor.20347)
31. Tinbergen J, Wilts BD, Stavenga DG. 2013 Spectral tuning of Amazon parrot feather coloration by psittacofulvin pigments and spongy structures. *J. Exp. Biol.* **216**, 4358–4364. (doi:10.1242/jeb.091561)
32. Bleiweiss R. 2014 Physical alignments between plumage carotenoid spectra and cone sensitivities in ultraviolet-sensitive (UVS) birds (Passerida: Passeriformes). *Evol. Biol.* **3**, 404–424. (doi:10.1007/s11692-014-9273-8)